RESEARCH ARTICLE

eGantryMate: A Piezo-Motor-Driven Lean and Flexible Assistance System for MR-Guided Interventions at 1.5T

SAMANTHA HICKEY [ID]1, **ALI C. ÖZEN** [ID]1, **(Senior Member, IEEE), SIMON REISS** [ID]1,
ANDREAS REICHERT1, **NIKLAS VERLOH** [ID]2, **THOMAS LOTTNER**1, **(Member, IEEE),**
SRDJAN MILOSAVLJEVIC3, **MICHAEL VOGELE**3, **WIBKE ULLER**2, **AND MICHAEL BOCK** [ID]1

1Division of Medical Physics, Department of Diagnostic and Interventional Radiology, University Medical Center Freiburg, Faculty of Medicine, University of Freiburg, 79106 Freiburg, Germany
2Department of Diagnostic and Interventional Radiology, University Medical Center Freiburg, Faculty of Medicine, University of Freiburg, 79106 Freiburg, Germany
3Interventional Systems GmbH, 6370 Kitzbühel, Austria

Corresponding author: Samantha Hickey (samantha.hickey@uniklinik-freiburg.de)

ABSTRACT In closed-bore MRI units, assistance systems play a crucial role in overcoming patient access limitations during percutaneous interventions. In this work, we present eGantryMate, a piezo-motor-driven assistance system specifically designed for MR-guided needle interventions in high-field MRI systems. eGantryMate consists of an instrument positioning unit and a control unit equipped with piezo motors, radiofrequency filters, and shielding. Paired with a real-time tracking sequence for automatic marker detection and projection of the instrument trajectory onto the MR image, eGantryMate enables precise and efficient needle interventions. Targeting experiments were performed by inserting a biopsy needle into a series of fiducial targets in a phantom, and usability experiments were conducted in vivo without needle insertion. The results show artifact-free MR imaging, minimal temperature rise on the instrument positioning unit, and precise targeting capabilities. These findings demonstrate eGantryMate's ability to perform real-time needle alignments and insertions within the magnet bore, highlighting its potential to enhance the acceptability and efficacy of MR-guided interventions.

INDEX TERMS MR-guided interventions, magnetic resonance imaging, interventional MRI devices.

I. INTRODUCTION

Image guidance is essential for percutaneous interventional procedures, such as needle biopsies, to ensure accurate target localization [1]. MRI, in particular, offers the advantage of continuous real-time monitoring and localization of both interventional tools and targets throughout the procedure, without the potential risks associated with ionizing

The associate editor coordinating the review of this manuscript and approving it for publication was Cristian A. Linte.

radiation [2], [3], [4]. Real-time tracking with good soft-tissue contrast is essential, especially for abdominal interventions where organ motion due to breathing, cardiac activity, and peristaltic movements can pose challenges [5]. Moreover, the functional imaging capabilities of MRI can be a valuable tool for monitoring the treatment progress and assessing outcomes [6]. Initially, this motivated the development of open-bore systems for MR-guided interventions, that would allow direct patient access during imaging [7]. These systems are, however, limited
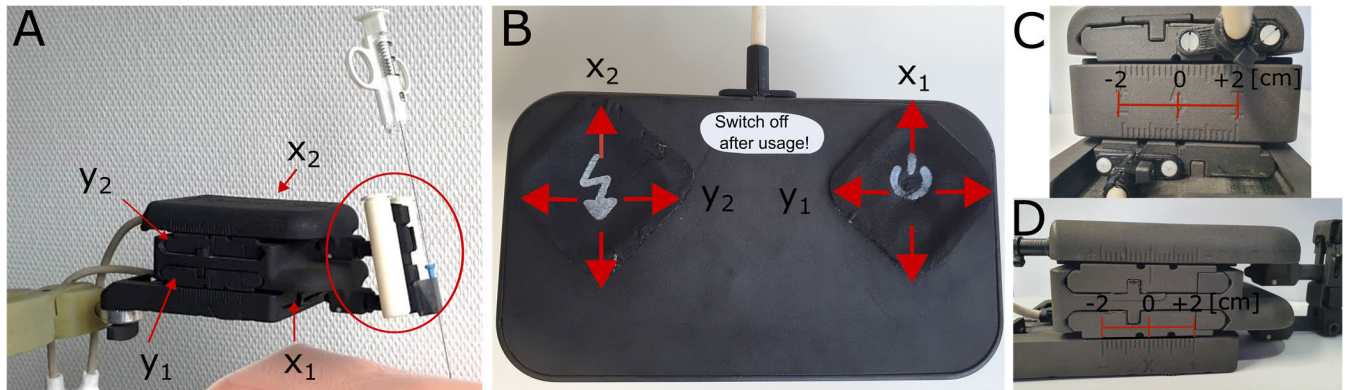
FIGURE 1. The eGantryMate instrument positioning unit (IPU) comprises four independently moving plates (A). The control unit (B) governs the movement of these four plates in either the x_1, y_1, y_2, and x_2 directions. This induces movement of the end-effector, depicted in (A), consisting of a needle guide and two markers. The translational motion range ($\pm$ 2 cm) and initial IPU position (C, D), which is visually re-aligned.

in the applicable field strength. Closed-bore systems, on the other hand, operating at higher field strengths limit patient access but provide a higher signal-to-noise ratio (SNR) and contrast-to-noise ratio (CNR) [1], which improves the identification and differentiation of lesions from healthy tissue. The optimal MRI system for interventional MRI is still debated [2], [6], [8], [9], but high-field closed-bore MRI systems are more widely available in clinical practice.

In closed-bore magnets, interventional procedures are prolonged due to the challenging patient access [10]. In shorter magnets with a wider diameter, it is easier to reach the patient. Recent developments of low-field closed-bore MRI systems were partly motivated to achieve larger bore diameters, i.e., 85 cm compared to 60-70 cm [11]. Nonetheless, in these large-diameter systems, it is still challenging for the operator to reach the region of interest inside the magnet bore, particularly during lengthy interventions or if the interventionalist has only a short arm length. Often, the patient must be repeatedly moved in and out of the bore. This necessitates continual readjustment and realignment of the imaging plane that contains the target of interest and the instrument. This workflow is both inefficient and cumbersome for clinicians and patients, thereby diminishing the clinical acceptance of MR-guided interventions.

Assistance systems designed for interventions in closed-bore MRI systems can overcome these problems by providing enhanced precision and reproducibility compared to free-hand approaches [12]. To be suitable for MR-guidance applications, assistance systems must be designed for safe use in the MR environment, i.e., they should be determined as MR safe or MR conditional according to American Society for Testing and Materials (ASTM) F2503-20 [13]. Furthermore, they should not significantly reduce the diagnostic quality of MR images or have their intended functionality degraded by the MRI system. MR safety requirements are regulated by international standards and guidelines [13], [14], [15]. To be intrinsically MR-safe, hydraulic [16], pneumatic [17], [18],

[19], [20], [21], [22], and remote-mechanical [23] actuators can be designed from non-magnetic components. One such example is the GantryMate assistance system (Interventional Systems, Kitzbühel, Austria), which is steered remotely using rotations of extension rods to manipulate the instrument's orientation and is composed solely of plastic components [23]. It thus facilitates the real-time adjustment of the needle orientation during MR-guided biopsies.

While the manual GantryMate system is mechanically simple and effective, an electronic actuation of the assistance system would reduce manual labor and improve the workflow by offering more intuitive input options to the operator. Various approaches, including pneumatics [24], [25], piezoelectric ultrasonic motors [26], [27], [28], MR-system-driven actuation [29], and more recently, servomotors [30], have been proposed for electronic actuation. Commercial robotic devices are often incompatible with MRI due to their ferromagnetic and magnetic materials. Therefore, pneumatic and piezoelectric actuator technologies are preferred for MRI applications [31], [32]. In the case of pneumatic actuators in MRI, long transmission lines are required, which can lead to mechanical instability and reduced precision due to potential oscillation and overshoot in the pistons [30], [33].

FIGURE 2. The experimental setup for phantom targeting. The instrument positioning unit (IPU) is positioned over the target region using a dedicated MR-conditional flexible holding arm.
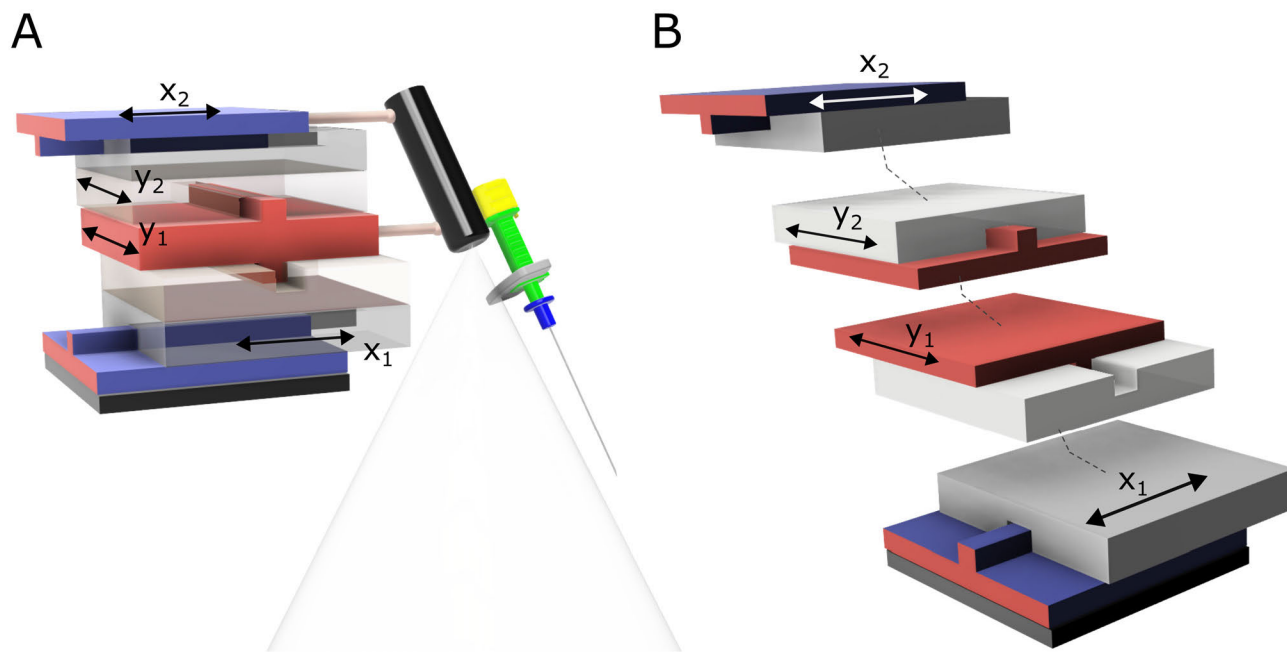
FIGURE 3. CAD model of the eGantryMate with four moving plates, two for translational positioning along x and y (x_1, y_1), and two for rotation of the needle holder around y and x axes (y_2, x_2) (A). The mechanical design is based on a commercially available device developed for CBCT-guided percutaneous interventions (Micromate^{TM}, Interventional Systems, Kitzbühel, Austria). Rotational plates are also displayed separately to highlight the respective positioning of the plates, which consist of a stationary and a moving pair (B). The resulting target volume is conical and can be displaced ± 20mm along the x and y directions.

Piezo-electric actuators are the preferred choice for lesion-targeting interventions because of their high geometric precision [34], [35], [36]. However, due to switching operations in control electronics and power networks, electrically controlled motors and actuators can generate unwanted electromagnetic interference (EMI) signals at a broad frequency range. The EMI is detected by the radiofrequency (RF) receive coils of the MRI system operating at the Larmor frequency, e.g., 64 MHz at 1.5 T and 128 MHz at 3 T, and manifests as zipper artifacts or an elevated noise floor. While electromagnetic compatibility (EMC) techniques have been effective in enhancing performance, they have also been reported to reduce the image signal-to-noise ratio (SNR) by 15–60% [34], [35], [36], [37].

In this work, we present a piezo-motor-driven, lean, and flexible assistance system, eGantryMate, which offers EMI-free operation during real-time MR-guided interventions. We combine eGantryMate with a passive real-time tracking sequence [38], [39] and demonstrate its targeting ability both *in vitro* and *in vivo*.

II. METHODS
A. eGantryMate ASSISTANCE SYSTEM
The assistance system, eGantryMate (Interventional Systems GmbH, Kitzbühel, Austria), comprises two main components: the control unit and the instrument positioning unit (IPU) (Fig. 1 and Fig. 2) [40], [41]. The mechanical design of the IPU is based on a commercially available device

originally developed for CBCT-guided percutaneous interventions (Micromate^{TM}, Interventional Systems, Kitzbuehel, Austria) [42], and on the purely mechanical MRI adapted version, GantryMate [23]. The eGantryMate IPU is equipped with four mobile plates, with two facilitating translational positioning along the x and y axes (x_1, y_1), and the remaining two enabling rotation of the end-effector around the y and x axes (y_2, x_2), as illustrated in Fig. 3. In Fig. 3b, the rotational plates are presented separately to highlight their positioning, consisting of both stationary and movable pairs. This configuration results in the end-effector, composed of a needle guide and two markers, having a conically shaped target volume that can be adjusted within a range of ± 20 mm along the x and y directions. An additional base stabilizing plate remains fixed in relation to the patient and is utilized for coarse positioning.

Manipulating each of the two plates controlling translational movement (x_1, y_1) results in a translational motion of ± 2 cm, while manipulating the top two plates (y_2, x_2) leads to a rotation of up to ± 27° of the end-effector. The initial position is calibrated by aligning the center markings on the IPU (Fig. 1). Supporting Information Fig. 1 provides a pictorial representation of the angular motion and Supporting Information Video 1 (2.5× speed) demonstrates the range of IPU movements.

The end-effector is equipped with two cylindrical passive markers for real-time tracking and an instrument holder. The instrument holder is compatible with commercially available
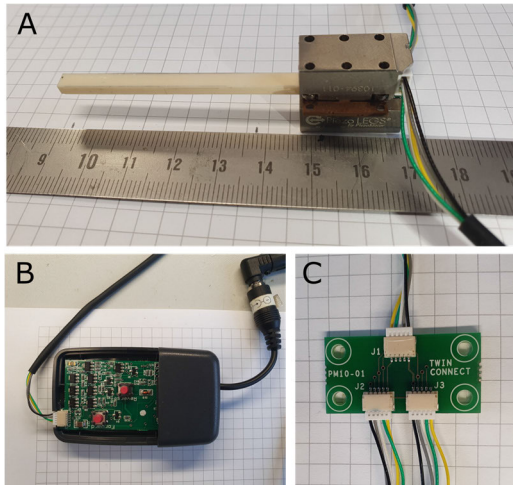
FIGURE 4. The commercially available piezo motors. (A) the piezo motor, (B) the controller, and (C) the connector board.

needle guides, which can be clipped into the holder. The complete eGantryMate assistance system weighs 2.2kg, of which 1kg is the control unit and 0.6kg is the IPU. The overall dimensions of the eGantryMate IPU and control unit are 21.2 × 8.5 × 7.0 cm and 21.0 × 12.0 × 8.5 cm, respectively.

The eGantryMate IPU has four integrated linear piezo motors, with two in each sliding plate. These piezo motors operate based on the inverse piezoelectric effect, wherein a material deforms under an electric voltage. In the IPU, we utilized commercially available piezo motors (Piezo LEGS, PiezoMotor, Sweden) equipped with bimorph layers (Fig.4). These layers extend and flex laterally to execute a walking-like movement. The non-magnetic motors weigh 29g, have a maximum velocity of 24 mm/s and a stall force of 20 N at an operation voltage of 42-48 V. The observed velocity was recorded during normal operation of the assembled eGantryMate device. The motors are operated from a control unit, which enables independent and concurrent movement of each plate. (Fig. 1). To avoid EMI from converter units, the device is powered by a rechargeable 12 V Li-ion battery.

B. EMI SUPPRESSION

Each piezo motor generates multiple sources of EMI: from the power supply, the control unit, and conducting connection cables that can pick up noise signals. These signals are then transmitted to the MRI's receive coils within the magnet. In addition to EMI from external sources, electromagnetic fields generated during RF pulses can couple to the conductors, resulting in common-mode currents. These currents may cause RF-induced heating or disrupt device functionality. To ensure that EMI signals do not contaminate the MRI signal and to prevent device malfunction, the following measures were implemented: (1) an RF shield enclosure, (2) harmonic suppression (HS) filters at the control signal paths, and (3) current traps.

For effective RF shielding, the entire control unit, which included the power supply, piezo motor drivers, and HS filters, was enclosed within a protective box (Fig. 1). This box was coated with conductive silver paint and fitted with copper tape segments. A shielded cable bundle was used to transmit the control signal and power to the piezo motors in the IPU. The cable bundle's shield was connected to that of the control unit to minimize the emission of EMI signals. At the output of the controller unit, HS filters were incorporated, specifically low-pass filters with a cutoff frequency of 3.1 MHz (Supporting Information Fig. 2). To suppress common-mode currents, floating current traps [43] were placed along the cable bundle at intervals of 80 cm. Finally, piezo motors, the piezoelectric material, and the sliding plates in the IPU were covered by conductive silver paint and galvanically connected to the shield of the cable bundle, thus completing the RF shielding enclosure.

C. DEVICE TRACKING

For real-time tracking of the needle-guide orientation, two contrast filled (Magnevist®/H_2O:1/200, Bayer Schering Pharma AG, Berlin, Germany) coaxial cylinders are attached to the end-effector. Each cylinder varies in size to enable robust identification and correct calculation of the end-effector directionality during the image reconstruction. The small and large cylinders have an inner diameter of 5 mm and 6.5 mm, and an outer diameter of 10 mm and 13 mm, respectively. A phase-only cross-correlation (POCC) tracking sequence was used to detect these markers, automatically identifying both cylinders [38], [39], [44], [45]. The sequence runs in a continuous feedback loop, initially acquiring two consecutive cross-sectional FLASH tracking images perpendicular to the cylinders (Fig. 5a). In both tracking images, the cylinders are identified as two rings with different diameters (Fig. 5a). The POCC template matching algorithm automatically determines the position of the rings in each tracking image, resulting in four positions.

These four positions allow calculation of a plane, which is shifted by 20 mm such that a targeting image can be acquired parallel to the needle guide (Fig. 5b). Following the two tracking images, a targeting image is acquired using a Balanced Steady State Free Precession (bSSFP) sequence. Each individual image acquisition, comprising of two FLASH images and one bSSFP image, takes approximately 0.5 seconds, depending on specific imaging parameters. Therefore, a complete tracking and targeting cycle provides a new frame with an updated position of the needle guide every 1.5 seconds (Fig. 5c).

To detect the MR-invisible needle tip position, a spherical marker filled with the same contrast agent solution is attached to the top of needle handle (Fig. 5d). In the targeting image, the marker is automatically detected using maximum intensity projection over a region of interest (ROI). The position is shifted by the known distance between the marker and the needle tip. This position is then superimposed onto the tracking image offering the operator a visualization of the
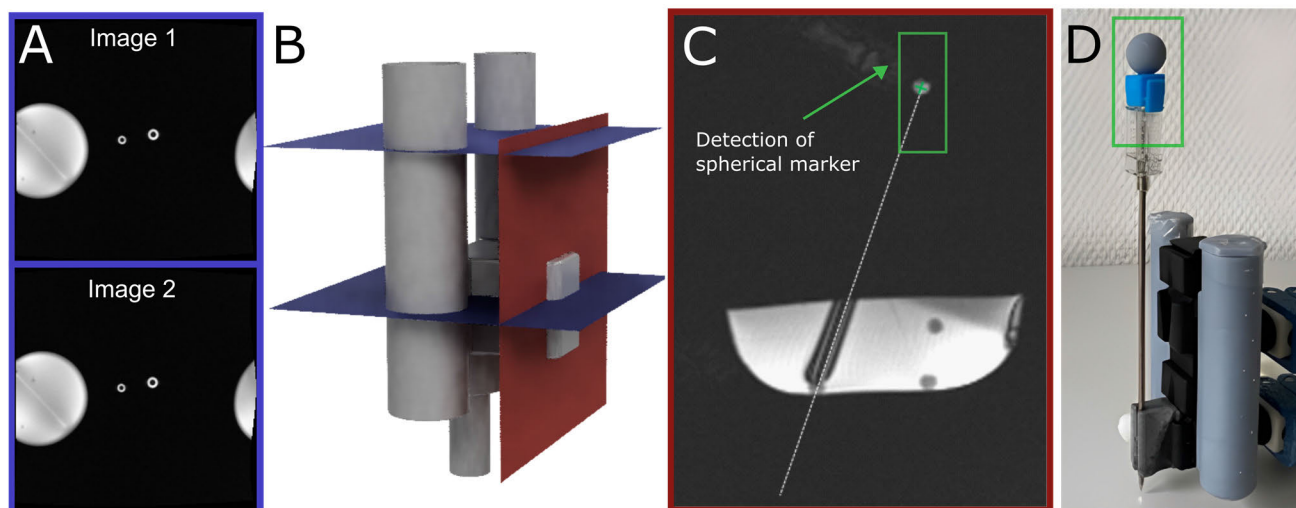
FIGURE 5. The POCC tracking sequence acquires two cross-sectional images (A, Image 1 and Image 2) through the end-effector as shown in B. Within these two images, the coaxial cylinders appear as discernible rings, which are then automatically detected using a POCC algorithm (A). One cylinder is slightly larger than the other cylinder, which ensures that the projected imaging plane for the needle is in the correct orientation during imaging, when the physical device cannot be visualized. (B) A spherical marker is placed on top of the needle to show the tip of the needle during targeting and biopsy. (C) The targeting slice during a phantom experiment, during needle insertion is shown. The spherical marker and the projected needle trajectory is also visible.
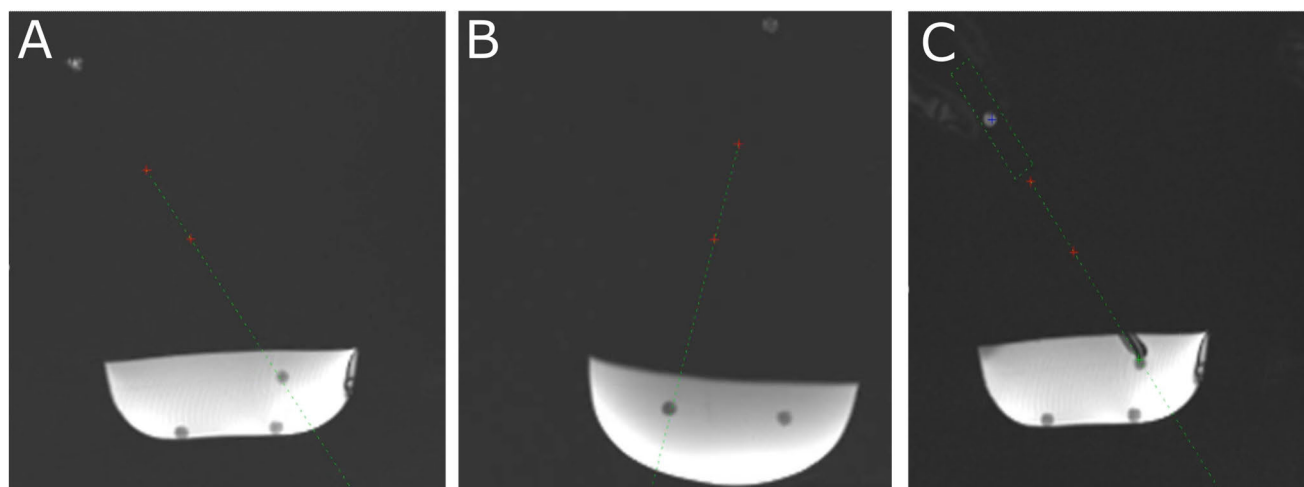
FIGURE 6. Phantom targeting experiments, where the needle trajectory is aligned first in a plane parallel to the cylinders (A) and secondly in a plane perpendicular to the cylinders to confirm alignment (B). Then, the needle is inserted (C). The needle tip estimation (green cross) as extra guidance.

needle's current depth within the tissue. The needle tip estimation was integrated into the feedback loop of the POCC tracking sequence.

D. MR SAFETY MEASUREMENTS

To validate the safe use of the eGantryMate under the tested conditions, we conducted evaluations focusing on magnetically-induced displacement forces, torque, MR image artifacts, and the device's overall temperature rise, in accordance with ASTM test guidelines [46]. To assess displacement force on the IPU unit the tests described in [47] were applied. The torque was evaluated by placing the IPU

unit on a rotating plate made from Polyvinyl Chloride (PVC) and moving the patient table in and out. Although the IPU unit is placed 2-3 cm away from the patient, a thermal camera (RS-700, RS Components GmbH, Frankfurt, Germany) was used to monitor the heating of the plates. Additionally, the cable from the control unit was measured during a 15-minute-long repetitive RF pulse (1 ms-long rectangular pulse, TR = 5 ms) exposure with a system-reported whole-body SAR of 3.2 W/kg. Finally, both gradient echo (GRE) and spin echo (SE) pulse sequences using the imaging parameters given in [48] were used to evaluate image artifacts. Here, measurements with active controllers and moving piezo

TABLE 1. Summary of time taken for in vivo targeting experiments.

Surrogate Targets	Parallel Orientation Time (seconds)	Perpendicular Orientation Time (seconds)	Time to switch sequence orientation (seconds)	Total targeting procedure time (seconds)
Spinal Cord	31	13	10	54
Bowl Section	26	15	10	51
Spinal Disc	31	4	66	101
Liver Vessel 1	23	12	9	44
Liver Vessel 2	32	11	10	53
Liver Vessel 3	31	21	108	160
Liver Vessel 4	25	4	12	41
Liver Vessel 5	39	9	21	69
Mean ± SD[a] (range)	29.8 ± 4.8 (23-39)	11.1 ± 5.3 (4-21)	30.8 ± 34.3 (9-108)	71.7 ± 37.9 (41-160)

[a] Respective mean values and standard deviations (SD) are summarized in the bottom line.

motors were compared to a reference measurement where the IPU was switched off and removed. Additionally, image artifacts were evaluated in the same manner for the tracking sequence.

E. TARGETING EXPERIMENTS

The targeting experiments were performed in a phantom on a clinical 1.5 T whole body system (Magnetom Aera, Siemens Healthineers, Erlangen, Germany) using a surface coil (Flex Large 4) for signal reception. The eGantryMate IPU was positioned above the phantom (Fig. 2) using a flexible holding arm (Interventional Systems GmbH, Kitzbühel, Austria). This flexible arm consists of aluminum, Ultem 9085, and plastic components. The design allows the variable positioning of the device on the patient table. Additionally, a specific spinal board is available, which provides more fixation locations for the flexible arm. The setup procedure for the support arm is available in Supporting Information Fig. 3. A gelatin phantom containing 12 fiducials (mean diameter: 7.6 mm) was used as a target for needle insertions. The real-time POCC tracking sequence was used to continually monitor the needle position while targeting.

The sequence parameters used were as follows: TR/TE = 3.4/1.5 ms, BW = 898 Hz/px, SL_{FLASH} = 10 mm, SL_{bSSFP} = 4.5 mm, FOV = 243 × 300 mm, matrix = 192 × 156, GRAPPA = 2, TA = 0.53 s, duration of full tracking cycle = 1.59 s (2 × FLASH + 1 bSSFP acquisition). During targeting the operator oriented the needle guide using the control unit until the projected trajectory was pointing at the pre-determined fiducial target. Next, the alignment was verified in a plane perpendicular to the first plane. Once the target was aligned, a 16 G needle (Somatex GmbH, Teltow) was inserted under continuous image guidance using the POCC sequence for needle tip visualization to estimate the insertion depth. After the needle was inserted, the lateral and longitudinal distances of the needle pathway to the geometric center of the fiducial was determined for each target using a high-resolution (0.5 × 0.5 × 0.5 mm) 3D GRE data set.

F. VOLUNTEER EXPERIMENTS

Targeting experiments were performed in a 1.5 T whole body system (Magnetom Avanto Fit, Siemens Healthineers, Erlangen, Germany) using a flexible coil (Flex Large 4, Siemens Healthineers) and a rigid spine coil array (Spine Matrix 32, Siemens Healthineers) for signal reception. Volunteer experiments were approved by the institutional
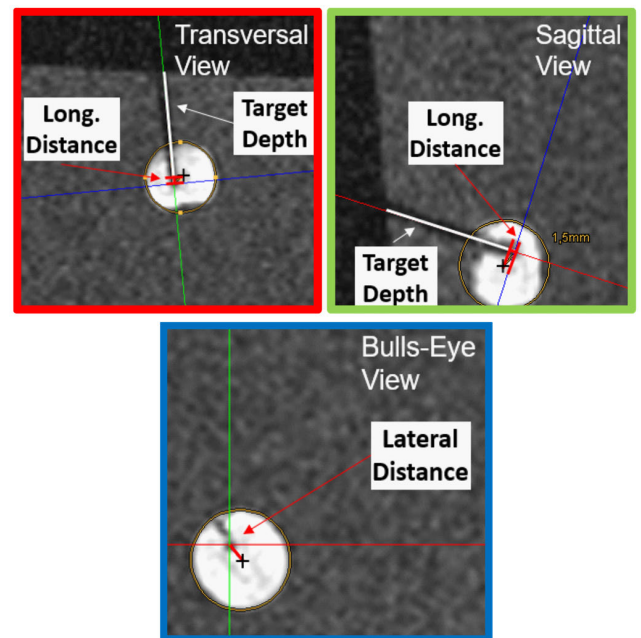
FIGURE 7. Evaluation of the accuracy by measuring the longitudinal (red, green) and lateral distance (blue) from the needle insertion point to the nominal center of the target.
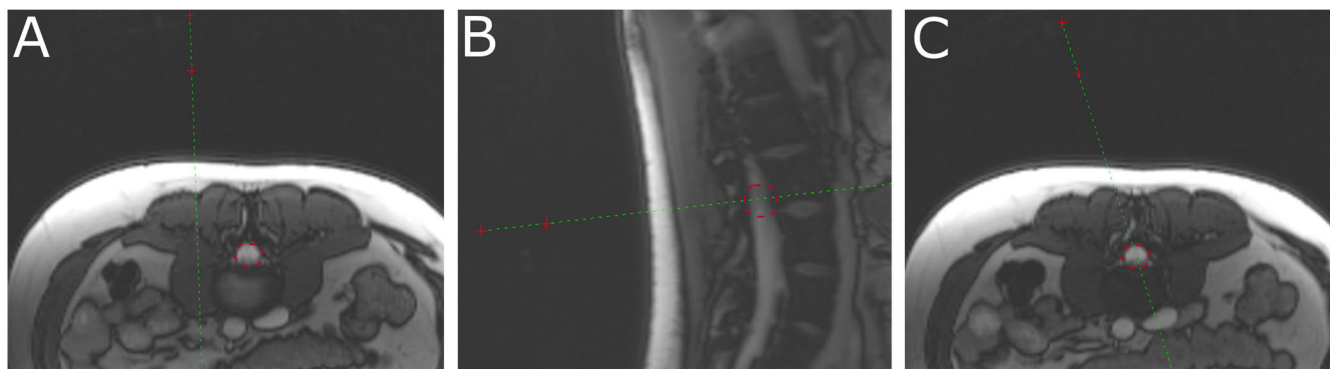
FIGURE 8. In vivo targeting experiment on the spinal cord as a surrogate target. (A) The initial position of the needle trajectory. (B) Targeting in a perpendicular plane. In (C), the projected needle pathway (indicated by a green-dashed line) is aligned in a predetermined spinal disc (indicated by a red-dashed contour).

review board (Ethik-Kommission) of the University Medical Center Freiburg (No. 160/2000). Informed written consent was obtained before imaging. The volunteer was positioned in the prone position, and the targeting of a biopsy procedure with in vivo needle guidance was simulated. To begin, a relatively stationary structure, such as the spinal cord, was defined as an artificial target. The targeting sequence provided real-time images throughout the orientation of the needle in a single plane.

The user moved the needle guide during continuous real-time imaging to align the needle trajectory with the target. The targeting sequence provided real-time images throughout the orientation of the needle in a single plane. The sequence was stopped and restarted to confirm the needle alignment in a second orthogonal plane. The time taken for targeting in each orientation, as well as switching imaging orientations was recorded for these experiments.

To simulate targeting of moving structures the same experiment was repeated in the abdomen and specifically targeting liver vessels, with the volunteer in the supine position. The initial targeting was performed while the volunteer was freely breathing, and then during final position alignment, the volunteer was asked to perform a short breathhold. The following parameters were used: FLASH tracking images: $\alpha_{FLASH} = 25°$, TR/TE = 3.48/1.55 ms, BW = 705 Hz/px, slice thickness = 10 mm, FOV = 375 mm × 375 mm, matrix = 154 × 192, partial Fourier = 6/8, TA = 0.4 s; bSSFP targeting image: $\alpha_{bSSFP} = 70°$, TR/TE = 3.48/1.55 ms, BW = 705 Hz/px, slice thickness = 6 mm, FOV = 375 mm × 375 mm, matrix = 154 × 192, partial Fourier = 6/8, TA = 0.4 s. The total acquisition time for each tracking cycle (two FLASH tracking slices and one bSSFP targeting slice) was 1.2 seconds.

III. RESULTS

While testing the safe use of the eGantryMate in MRI, the incorporation of HS filters achieved a suppression of 78 dB at 64 ± 0.5 MHz. Additionally, the integration of floating current traps resulted in a suppression of common-mode currents of 27 ± 4 dB between the control unit and the IPU. No magnetic displacement force or torque was measurable in the IPU. The maximum temperature rise on the IPU surface was less than 0.4°C. The highest temperature rise of 1.5°C was measured on the current trap located before the control signal splitter in front of the IPU. SNR reduction during activity of the eGantryMate system was less than 7.8 %, 4.5 %, and 5.3 % compared to reference images for GRE, SE, and POCC tracking sequences, respectively.

The velocity of the piezo motors during device operation was recorded at 1.5 mm/s and 2.5 mm/s for the x_1, and y_1 translational plates, respectively. Additionally, the velocity of the top two rotational movement plates, y_2, and x_2, was measured at 4.3 mm/s and 4.9 mm/s, respectively.

Targeting experiments could be completed successfully in all 12 fiducial markers using the combination of the eGantryMate and the POCC tracking sequence (Fig. 6). The target diameter measured on average as 7.6 ± 0.5 mm (Fig. 7) [40]. The lateral distance and longitudinal distance between the needle insertion point and the nominal center of the target were measured as 1.3 ± 0.8 mm and 1.8 ± 0.8 mm, respectively (Fig. 7). Overall, the mean total procedure time (instrument positioning + needle insertion) was 4.3 ± 1.2 min.

The eGantryMate assistance system and the POCC tracking sequence effectively visualized and targeted predetermined surrogate structures, such as the liver vessels and spine discs (Fig. 8 and 9). The average time for targeting in the first imaging orientation was 29.8 ± 4.8 seconds and 11.1 ± 5.3 seconds in the second orientation. The average time to switch between the two orthogonal imaging orientations was 30.8 ± 34.3 seconds (Table 1). Finally, the total average time from the beginning of the sequence until the projection was aligned with the target was 71.1 ± 37.9 s.

IV. DISCUSSION

In this work, a piezo-motor-driven assistance system, eGantryMate, was evaluated for safe use in MRI and combined with a real-time POCC based tracking sequence for
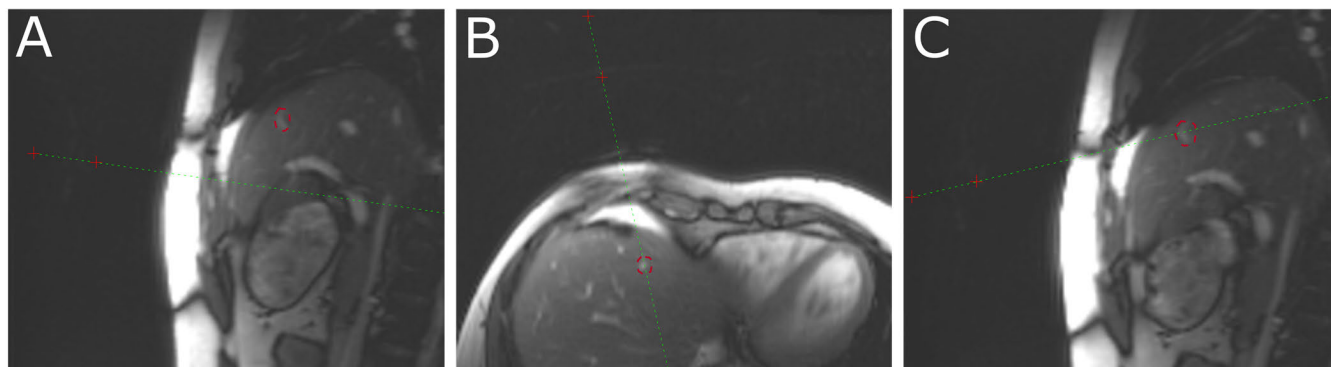
FIGURE 9. In vivo targeting experiment on a liver vessel. (A) The initial position of the needle trajectory in the liver. (B) Demonstrates targeting in a perpendicular plane. In (C), the projected needle pathway (indicated by a green-dashed line) is aligned in a predetermined liver vessel (indicated by a red-dashed contour).

MR-guided needle interventions. The integrated piezoelectric motors drive the motion in the x_1, y_1, y_2, and x_2 sliding plates of the IPU, providing translational and rotational motion of the end-effector and, hence, ultimately the attached instrument. The eGantryMate assistance system combined with the POCC sequence successfully targeted 12 fiducial markers in phantom experiments. Moreover, we demonstrated the ability of the system to target several surrogate structures both in the spine and liver in *in vivo* targeting simulation experiments.

The procedure workflow and the handling of the assistance system was very intuitive, and the setup was both ergonomic and user-friendly so that even for inexperienced users no additional training was required. In the *in vivo* experiments the patient was either in a supine or prone position on the MRI table, while the IPU was coarsely positioned near the pre-defined target area, supported by dedicated MR-conditional supporting arms (Fig. 2). The interventionalist stands next to the patient table, from which they observe the real-time images on separate in-room monitor and orient and pre-cisely position the needle. This workflow is similar to other MR-guided interventions and gives the interventionalist full control over the assistance system, but also allows removal of the patient rapidly from the magnet if unexpected events occur.

Compared to the previous mechanical version [23] where translation and rotation of the end-effector were performed manually by turning rods connected to the system, in this new electric version, the manipulation of the end-effector is possible only using a small control unit. The intuitive nature of eGantryMate's design potentially provides a further advan-tage, as a technician could complete the time-consuming initial targeting and positioning of the needle, and clinicians would only have to confirm the positioning and perform the percutaneous needle insertion. This could streamline the MR-guided needle interventions, allowing for improved workflows.

While the current system is designed for interventions where the clinician remains inside the MR room to have complete control over the procedure, it would be possible to place the control unit in the MR control room, which would enable remote operation from the MR console. Furthermore, the design of the currently wired system could be altered to include a wireless connection link between the IPU and the control unit.

Incorporating both HS filters with very high suppression rates and continuous RF shielding from source to the ceramic rods of the IPU by applying conductive paint resulted in effec-tive EMI suppression. Compared to other piezo-motor-driven electronic actuators, a substantially lower reduction in SNR in the range of 5-8% was observed [34], [35], [36]. Recently, nonmagnetic servomotors that use the B_0 field of the MRI system for rotation have been proposed as an alternative [30]. Although the EMC performance of the servomotors during MRI is promising, their function and performance depend on the orientation and position of the motor in relation to B_0, which adds additional challenges to implement a full scale multi-axes IPU. Thus, the presented solution with piezo motors is more flexible.

The results on EMC and MR-safety are valid only for the tested field strength and the corresponding ^{1}H Larmor fre-quency, i.e., 63.87 MHz for 1.5T. For other magnetic fields, the EMI suppression units such as HS filters and BALUNs must be adapted to the corresponding Larmor frequency. In addition, the shielding might need to be redesigned for sim-ilar performance, as shielding effectiveness might be reduced at higher frequencies.

Currently, the POCC tracking sequence not only sup-ports a bSSFP contrast for the targeting plane but also includes a FLASH contrast option. The latter proves bene-ficial when banding artifacts interfere with visualizing the targeting region. The tracking sequence, however, is only capable of acquiring images in a single plane. While the average total targeting time only 71.7 $\pm$ 37.9 s demon-strates that with the assistance system needle targeting can be performed in approximately one minute, the acquisition of the first orientation took longer compared to the second orientation. This occurs because the needle pathway had already been aligned with the target during the first orien-

tation and only minor corrections are required. The average time required to switch between the two imaging planes was approximately 30 s. This duration could potentially be reduced by using a sequence that can visualize two orthogonal slices simultaneously. A similar interchangeability in contrast of the sequences could be obtained with simultaneous orthogonal lice sequences, for example, with a T1-weighted gradient echo [49], [50] or T2-weighted SSFP-echo [51] contrast. Multiple contrast options could again allow better visualization during targeting and insertion. These sequences produce a saturation band in the slice overlap region, which in preliminary tests, did not inhibit the visualization of needle insertion, as the artifact was substantially larger than the 5 mm saturation band.

In image-guided needle biopsies, respiratory motion continues to pose a significant challenge. Faster image acquisition methods are beneficial as they require shorter breath-holds, which increases patient compliance. The POCC sequence can be accelerated using techniques like partial Fourier acquisition and parallel imaging. However, parallel imaging requires careful consideration of both the phase encoding direction and the coil setup, which can be challenging in interventional procedures where the slice orientation is changing. Alternatively, dedicated targeted image acquisition methods could be used to shorten the acquisition time, which employ saturation pulses for outer volume suppression [52] or inner-volume excitation HASTE [53] thus reducing the field of view. These methods could be helpful during needle insertion but might not be applicable during alignment of the needle as this requires a good overview over the anatomy.

The previous version of the POCC was limited to detecting a single cylindrical marker which also functioned as a needle guide. However, needles create significant artifacts in the image of the cylinder cross section making the POCC position detection less precise, which is especially challenging during the most critical phase of the intervention -the needle insertion.

This limitation was mitigated by incorporating a second cylinder and moving both cylinders out of the plane of the needle. The shift facilitates the visualization of needle insertion during real-time imaging, and it also allows for the use of larger needles as they do not have to be introduced through the marker. In addition, the two markers allow to align the imaging slice with the motion axes of the device which renders the operation more intuitive.

In summary, despite these modifications the mean total procedure time in phantom experiments (instrument positioning + needle insertion) of 4.3 ± 1.2 min was comparable to that of previous studies [38], [39], [54].

A limitation of our *in vivo* study is that targeting experiments were performed without actual needle insertions. To assess the effectiveness of the assistance system, pre-clinical and clinical studies should be conducted with MR conditional biopsy needles. Furthermore, the workflow needs

to be optimized; for example, following coarse positioning of the assistance system on the patient, a 3D scan is taken to localize and define the target so that the POCC targeting can be started. During POCC imaging the noise generated by the sequence may hinder effective communication with both the patient and the staff in the room, which can be solved using dedicated communication systems for use in MRI.

V. CONCLUSION

The eGantryMate assistance system was realized by incorporating MR conditional piezoelectric stepper motors to create translational and rotational motion of a distal end-effector. In the experiments, no signal interference or substantial heating was observed, all the 7.6 mm fiducial targets were successfully punctured, and the needle trajectory was aligned with a target in volunteer experiments. The proposed eGantryMate system could increase the clinical acceptance of MR-guided percutaneous needle interventions by improving the user experience and intuitiveness and reducing manual manipulation.

REFERENCES

[1] C. R. Weiss, S. G. Nour, and J. S. Lewin, "MR-guided biopsy: A review of current techniques and applications," *J. Magn. Reson. Imag.*, vol. 27, no. 2, pp. 311–325, Feb. 2008, doi: 10.1002/jmri.21270.

[2] E. A. Kaye, K. L. Granlund, E. A. Morris, M. Maybody, and S. B. Solomon, "Closed-bore interventional MRI: Percutaneous biopsies and ablations," *Amer. J. Roentgenol.*, vol. 205, no. 4, pp. 400–410, Oct. 2015, doi: 10.2214/ajr.15.14732.

[3] C. R. Weiss and J. Fritz, "The state-of-the-art of interventional magnetic resonance imaging: Part 2," *Topics Magn. Reson. Imag.*, vol. 27, no. 3, pp. 113–114, 2018. [Online]. Available: https://journals.lww.com/topicsinmri/Fulltext/2018/02000/The_State_of_the_Art_of_Interventional_Magnetic.2.aspx

[4] M. Bock and F. K. Wacker, "MR-guided intravascular interventions: Techniques and applications," *J. Magn. Reson. Imag.*, vol. 27, no. 2, pp. 326–338, Feb. 2008, doi: 10.1002/jmri.21271.

[5] J. Tokuda, L. Chauvin, B. Ninni, T. Kato, F. King, K. Tuncali, and N. Hata, "Motion compensation for MRI-compatible patient-mounted needle guide device: Estimation of targeting accuracy in MRI-guided kidney cryoablations," *Phys. Med. Biol.*, vol. 63, no. 8, Apr. 2018, Art. no. 085010, doi: 10.1088/1361-6560/aab736.

[6] A. E. Campbell-Washburn, R. Ramasawmy, M. C. Restivo, I. Bhattacharya, B. Basar, D. A. Herzka, M. S. Hansen, T. Rogers, W. P. Bandettini, D. R. McGuirt, and C. Mancini, "Opportunities in interventional and diagnostic imaging by using high-performance low-field-strength MRI," *Radiology*, vol. 293, no. 2, pp. 384–393, Nov. 2019, doi: 10.1148/radiol.2019190452.

[7] J. F. Schenck, F. A. Jolesz, P. B. Roemer, H. E. Cline, W. E. Lorensen, R. Kikinis, S. G. Silverman, C. J. Hardy, W. D. Barber, E. T. Laskaris, and B. Dorri, "Superconducting open-configuration MR imaging system for image-guided therapy," *Radiology*, vol. 195, no. 3, pp. 805–814, Jun. 1995, doi: 10.1148/radiology.195.3.7754014.

[8] A. C. Ozen, M. F. Russe, T. Lottner, S. Reiss, S. Littin, M. Zaitsev, and M. Bock, "RF-induced heating of interventional devices at 23.66 MHz," *Magn. Reson. Mater. Phys., Biol. Med.*, vol. 36, no. 3, pp. 439–449, 2023, doi: 10.1007/s10334-023-01099-7.

[9] F. Sedaghat and K. Tuncali, "Enabling technology for MRI-guided intervention," *Topics Magn. Reson. Imag.*, vol. 27, no. 1, pp. 5–8, Feb. 2018, doi: 10.1097/rmr.0000000000000148.

[10] S. G. Hushek, A. J. Martin, M. Steckner, E. Bosak, J. Debbins, and W. Kucharzyk, "MR systems for MRI-guided interventions," *J. Magn. Reson. Imag.*, vol. 27, no. 2, pp. 253–266, Feb. 2008, doi: 10.1002/jmri.21269.

[11] M. Hamilton-Basich, "FDA clears siemens healthineers magnetom free.max 80 cm MR scanner," *AXIS Imaging News*, 2021. [Online]. Available: https://www.proquest.com/scholarly-journals/fda-clears-siemens-healthineers-magnetom-free-max/docview/2548999158/se-2

[12] W. J. Heerink, S. J. S. Ruiter, J. P. Pennings, B. Lansdorp, R. Vliegenthart, M. Oudkerk, and K. P. de Jong, "Robotic versus freehand needle positioning in CT-guided ablation of liver tumors: A randomized controlled trial," *Radiology*, vol. 290, no. 3, pp. 826–832, Mar. 2019, doi: 10.1148/radiol.2018181698.

[13] American Society for Testing and Materials. *Standard Practice For Marking Medical Devices and Other Items for Safety in the Magnetic Resonance Environment*, Standard ASTM F2503, 2020.

[14] International Electrotechnical Commission. *Medical Electrical Equipment—Part 2–33: Particular Requirements for the Safety of Magnetic Resonance Diagnostic Devices*, Standard IEC 60601-2-33, 2015.

[15] *Assessment of the Safety of Magnetic Resonance Imaging for Patients With an Active Implantable Medical Device*, Standard ISO 10974, 2018.

[16] Z. Dong, Z. Guo, K.-H. Lee, G. Fang, W. L. Tang, H.-C. Chang, D. T. M. Chan, and K.-W. Kwok, "High-performance continuous hydraulic motor for MR safe robotic teleoperation," *IEEE Robot. Autom. Lett.*, vol. 4, no. 2, pp. 1964–1971, Apr. 2019, doi: 10.1109/LRA.2019.2899189.

[17] Y. Chen, K.-W. Kwok, and Z. T. H. Tse, "An MR-conditional high-torque pneumatic stepper motor for MRI-guided and robot-assisted intervention," *Ann. Biomed. Eng.*, vol. 42, no. 9, pp. 1823–1833, Sep. 2014, doi: 10.1007/s10439-014-1049-x.

[18] D. B. Comber, J. E. Slightam, V. R. Gervasi, J. S. Neimat, and E. J. Barth, "Design, additive manufacture, and control of a pneumatic MR-compatible needle driver," *IEEE Trans. Robot.*, vol. 32, no. 1, pp. 138–149, Feb. 2016, doi: 10.1109/TRO.2015.2504981.

[19] J. G. R. Bomers, D. G. H. Bosboom, G. H. Tigelaar, J. Sabisch, J. J. Fütterer, and D. Yakar, "Feasibility of a 2nd generation MR-compatible manipulator for transrectal prostate biopsy guidance," *Eur. Radiol.*, vol. 27, no. 4, pp. 1776–1782, Apr. 2017, doi: 10.1007/s00330-016-4504-2.

[20] D. Stoianovici, C. Kim, D. Petrisor, C. Jun, S. Lim, M. W. Ball, A. Ross, K. J. Macura, and M. E. Allaf, "MR safe robot, FDA clearance, safety and feasibility of prostate biopsy clinical trial," *IEEE/ASME Trans. Mechatronics*, vol. 22, no. 1, pp. 115–126, Feb. 2017, doi: 10.1109/TMECH.2016.2618362.

[21] V. Groenhuis, J. Veltman, F. J. Siepel, and S. Stramigioli, "Stormram 3: A magnetic resonance imaging-compatible robotic system for breast biopsy," *IEEE Robot. Autom. Mag.*, vol. 24, no. 2, pp. 34–41, Jun. 2017, doi: 10.1109/MRA.2017.2680541.

[22] V. Groenhuis, F. J. Siepel, J. Veltman, J. K. van Zandwijk, and S. Stramigioli, "Stormram 4: An MR safe robotic system for breast biopsy," *Ann. Biomed. Eng.*, vol. 46, no. 10, pp. 1686–1696, Oct. 2018, doi: 10.1007/s10439-018-2051-5.

[23] A. Reichert, M. Bock, M. Vogele, and A. J. Krafft, "GantryMate: A modular MR-compatible assistance system for MR-guided needle interventions," *Tomography*, vol. 5, no. 2, pp. 266–273, Jun. 2019, doi: 10.18383/j.tom.2019.00007.

[24] A. J. Krafft, J. W. Jenne, F. Maier, R. J. Stafford, P. E. Huber, W. Semmler, and M. Bock, "A long arm for ultrasound: A combined robotic focused ultrasound setup for magnetic resonance-guided focused ultrasound surgery," *Med. Phys.*, vol. 37, no. 5, pp. 2380–2393, May 2010, doi: 10.1118/1.3377777.

[25] A. Melzer, B. Gutmann, T. Remmele, R. Wolf, A. Lukoscheck, M. Bock, H. Bardenheuer, and H. Fischer, "INNOMOTION for percutaneous image-guided interventions," *IEEE Eng. Med. Biol. Mag.*, vol. 27, no. 3, pp. 66–73, May 2008, doi: 10.1109/EMB.2007.910274.

[26] S.-E. Song, J. Tokuda, K. Tuncali, C. M. Tempany, E. Zhang, and N. Hata, "Development and preliminary evaluation of a motorized needle guide template for MRI-guided targeted prostate biopsy," *IEEE Trans. Biomed. Eng.*, vol. 60, no. 11, pp. 3019–3027, Nov. 2013, doi: 10.1109/TBME.2013.2240301.

[27] N. A. Patel, C. J. Nycz, P. A. Carvalho, K. Y. Gandomi, R. Gondokaryono, G. Li, T. Heffter, E. C. Burdette, J. G. Pilitsis, and G. S. Fischer, "An integrated robotic system for MRI-guided neuroablation: Preclinical evaluation," *IEEE Trans. Biomed. Eng.*, vol. 67, no. 10, pp. 2990–2999, Oct. 2020, doi: 10.1109/TBME.2020.2974583.

[28] K. Masamune, E. Kobayashi, Y. Masutani, M. Suzuki, T. Dohi, H. Iseki, and K. Takakura, "Development of an MRI-compatible needle insertion manipulator for stereotactic neurosurgery," *J. Image Guid. Surg.*, vol. 1, no. 4, pp. 242–248, 1995, doi: 10.1002/(SICI)1522-712X(1995)1:4<242::AID-IGS7>3.0.CO;2-A.

[29] P. Vartholomeos, C. Bergeles, L. Qin, and P. E. Dupont, "An MRI-powered and controlled actuator technology for tetherless robotic interventions," *Int. J. Robot. Res.*, vol. 32, no. 13, pp. 1536–1552, Oct. 2013, doi: 10.1177/0278364913500362.

[30] L. W. Hofstetter, J. R. Hadley, R. Merrill, H. Pham, G. C. Fine, and D. L. Parker, "MRI-compatible electromagnetic servomotor for image-guided medical robotics," *Commun. Eng.*, vol. 1, no. 1, p. 4, May 2022, doi: 10.1038/s44172-022-00001-y.

[31] R. Monfaredi, K. Cleary, and K. Sharma, "MRI robots for needle-based interventions: Systems and technology," *Ann. Biomed. Eng.*, vol. 46, no. 10, pp. 1479–1497, Oct. 2018, doi: 10.1007/s10439-018-2075-x.

[32] G. S. Fischer, G. Cole, and H. Su, "Approaches to creating and controlling motion in MRI," in *Proc. Annu. Int. Conf. IEEE Eng. Med. Biol. Soc.*, Aug. 2011, pp. 6687–6690, doi: 10.1109/IEMBS.2011.6091649.

[33] B. Yang, U.-X. Tan, A. B. McMillan, R. Gullapalli, and J. P. Desai, "Design and control of a 1-DOF MRI-compatible pneumatically actuated robot with long transmission lines," *IEEE/ASME Trans. Mechatronics*, vol. 16, no. 6, pp. 1040–1048, Dec. 2011, doi: 10.1109/TMECH.2010.2071393.

[34] H. Elhawary, A. Zivanovic, M. Rea, B. Davies, C. Besant, D. McRobbie, N. de Souza, I. Young, and M. Lamperth, "The feasibility of MR-image guided prostate biopsy using piezoceramic motors inside or near to the magnet isocentre," in *Proc. Int. Conf. Med. Image Comput. Comput.-Assist. Intervent.*, 2006, pp. 519–526.

[35] G. S. Fischer, A. Krieger, I. Iordachita, C. Csoma, L. L. Whitcomb, and G. Fichtinger, "MRI compatibility of robot actuation techniques—A comparative study," in *Proc. Int. Conf. Med. Image Comput. Comput.-Assist. Intervent.*, 2008, pp. 509–517.

[36] A. Krieger, S.-E. Song, N. B. Cho, I. I. Iordachita, P. Guion, G. Fichtinger, and L. L. Whitcomb, "Development and evaluation of an actuated MRI-compatible robotic system for MRI-guided prostate intervention," *IEEE/ASME Trans. Mechatronics*, vol. 18, no. 1, pp. 273–284, Feb. 2013, doi: 10.1109/TMECH.2011.2163523.

[37] G. Li, H. Su, G. A. Cole, W. Shang, K. Harrington, A. Camilo, J. G. Pilitsis, and G. S. Fischer, "Robotic system for MRI-guided stereotactic neurosurgery," *IEEE Trans. Biomed. Eng.*, vol. 62, no. 4, pp. 1077–1088, Apr. 2015, doi: 10.1109/TBME.2014.2367233.

[38] A. Reichert, M. Bock, S. Reiss, C. G. Overduin, J. J. Fütterer, and A. J. Krafft, "Simultaneous slice excitation for accelerated passive marker tracking via phase-only cross correlation (POCC) in MR-guided needle interventions," *Magn. Reson. Mater. Phys., Biol. Med.*, vol. 31, no. 6, pp. 781–788, Dec. 2018, doi: 10.1007/s10334-018-0701-0.

[39] A. J. Krafft, P. Zamecnik, F. Maier, A. de Oliveira, P. Hallscheidt, H.-P. Schlemmer, and M. Bock, "Passive marker tracking via phase-only cross correlation (POCC) for MR-guided needle interventions: Initial in vivo experience," *Phys. Medica*, vol. 29, no. 6, pp. 607–614, Nov. 2013, doi: 10.1016/j.ejmp.2012.09.002.

[40] A. Reichert, "eGantryMate: A piezo-motor driven assistance system," in *Proc. Int. Soc. Mag. Reson. Med.*, vol. 31, Toronto, ON, Canada, Jun. 2023. [Online]. Available: https://cds.ismrm.org/protected/23MPresentations/abstracts/0751.html

[41] A. Reichert, "A piezo-driven MR-compatible assistance system for image-guided interventions (eGantryMate)," in *Proc. 13th Interventional MRI Symp.*, Leipzig, Germany, Oct. 2022, p. 41. [Online]. Available: https://www.imri2020.org/

[42] Y. Özbek, M. Vogele, C. Plattner, P. Costa, M. Griesser, and M. Wieczorek, "Fluoroscopy-guided robotic biopsy intervention system," *Current Directions Biomed. Eng.*, vol. 6, no. 1, Sep. 2020, Art. no. 20200020, doi: 10.1515/cdbme-2020-0020.

[43] D. A. Seeber, J. Jevtic, and A. Menon, "Floating shield current suppression trap," *Concepts Magn. Reson. B, Magn. Reson. Eng.*, vol. 21B, no. 1, pp. 26–31, Apr. 2004, doi: 10.1002/cmr.b.20008.

[44] P. Zamecnik, M. G. Schouten, A. J. Krafft, F. Maier, H.-P. Schlemmer, J. O. Barentsz, M. Bock, and J. J. Fütterer, "Automated real-time needle-guide tracking for fast 3-T MR-guided transrectal prostate biopsy: A feasibility study," *Radiology*, vol. 273, no. 3, pp. 879–886, Dec. 2014, doi: 10.1148/radiol.14132067.

[45] A. Reichert, S. Reiss, A. J. Krafft, and M. Bock, "Passive needle guide tracking with radial acquisition and phase-only cross-correlation," *Magn. Reson. Med.*, vol. 85, no. 2, pp. 1039–1046, Feb. 2021, doi: 10.1002/mrm.28448.

[46] ASTM International. *Standard Test Method for Measurement of Radio Frequency Induced Heating on or Near Passive Implants During Magnetic Resonance Imaging*, Standard F2182-19e2, West Conshohocken, PA, USA, 2020. [Online]. Available: https://www.astm.org/f2182-19e02.html

[47] ASTM International. *Standard Test Method for Measurement of Magnetically Induced Displacement Force on Medical Devices in the Magnetic Resonance Environment*, Standard F2052, West Conshohocken, PA, USA, 2006. [Online]. Available: https://www.astm.org/f2052-06.html

[48] ASTM International. *Standard Test Method for Evaluation of MR Image Artifacts from Passive Implants*. Standard F2119, West Conshohocken, PA, USA, 2013. [Online]. Available: https://www.astm.org/f2119-07r13.html

[49] A. J. Krafft, J. Rauschenberg, F. Maier, J. W. Jenne, and M. Bock, "Crushed rephased orthogonal slice selection (CROSS) for simultaneous acquisition of two orthogonal proton resonance frequency temperature maps," *J. Magn. Reson. Imag.*, vol. 38, no. 6, pp. 1510–1520, Dec. 2013, doi: 10.1002/jmri.24118.

[50] N. J. Mickevicius and E. S. Paulson, "Simultaneous orthogonal plane imaging," *Magn. Reson. Med.*, vol. 78, no. 5, pp. 1700–1710, Nov. 2017, doi: 10.1002/mrm.26555.

[51] S. Hickey, A. Reichert, W. Ptacek, L. Bielak, S. Reiss, J. Fischer, D. D. Gunashekar, T. Bortfeld, and M. Bock, "Simultaneous T_2-weighted real-time MRI of two orthogonal slices," *Magn. Reson. Med.*, vol. 90, no. 6, pp. 2388–2399, 2023, doi: 10.1002/mrm.29795.

[52] J. Rauschenberg, A. J. Krafft, F. Maier, P. Zamecnik, W. Semmler, and M. Bock, "Outer volume suppression in steady state sequences (OVSuSS) for percutaneous interventions," *Magn. Reson. Med.*, vol. 66, no. 1, pp. 123–134, Jul. 2011, doi: 10.1002/mrm.22789.

[53] H. Zimmermann, S. Müller, B. Gutmann, H. Bardenheuer, A. Melzer, R. Umathum, W. Nitz, W. Semmler, and M. Bock, "Targeted-HASTE imaging with automated device tracking for MR-guided needle interventions in closed-bore MR systems," *Magn. Reson. Med.*, vol. 56, no. 3, pp. 481–488, Sep. 2006, doi: 10.1002/mrm.20983.

[54] A. de Oliveira, J. Rauschenberg, D. Beyersdorff, W. Semmler, and M. Bock, "Automatic passive tracking of an endorectal prostate biopsy device using phase-only cross-correlation," *Magn. Reson. Med.*, vol. 59, no. 5, pp. 1043–1050, May 2008, doi: 10.1002/mrm.21430.

ALI C. ÖZEN (Senior Member, IEEE) was born in Turkey, in 1988. He received the bachelor's and master's degrees in electrical and electronics engineering from Bilkent University, Ankara, in 2011 and 2013, respectively, and the Ph.D. degree from the Institute of Microstructure Technology, Karlsruhe Institute of Technology, Germany, in 2017.

In 2013, he joined the Department of Radiology, Medical Physics, University Medical Center Freiburg, as a Research Assistant, where became a Postdoctoral Fellow, in 2017. From 2017 to 2021, he was a Scientist with German Consortium for Translational Cancer Research Partner Site Freiburg. He is currently an Engineer and the Head of the RF Laboratory, Division of Medical Physics, University Medical Center Freiburg. He is involved in scientific research and technology development in the fields of magnetic resonance imaging, cardiovascular interventions, and MR safety.

Dr. Özen is a member of the International Society of Magnetic Resonance in Medicine and a School of Oncology Fellow of German Cancer Research Center (DKFZ). He was a recipient of the Young Investigator Award from European Society of Magnetic Resonance in Medicine and Biology, in 2015. In 2019, he received the Lasby Fellowship from the University of Minnesota.

SIMON REISS was born in Freiburg, Germany, in 1989. He received the bachelor's and master's degrees in physics from the University of Freiburg, in 2011 and 2014, respectively, and the Ph.D. degree from the Department of Radiology, Medical Physics, University Medical Center Freiburg, with a focus on MR-guided interventions and MR safety.

Since 2021, he has been a Postdoctoral Fellow in the field of interventional and cardiac MRI. He is a member of the International Society of Magnetic Resonance in Medicine.

SAMANTHA HICKEY was born in Townsville, Australia, in 1995. She received the bachelor's degree in electrical and electronic engineering from James Cook University, Townsville, in 2016, and the M.A.Sc. degree in medical physics from the Queensland University of Technology, Brisbane, QLD, USA, in 2020. She is currently pursuing the Ph.D. degree with the Department of Interventional Radiology, Medical Physics, University Medical Center Freiburg.

She is with the University Medical Center Freiburg, where she is involved in MR-guided interventions. She is a member of the International Society of Magnetic Resonance in Medicine.

ANDREAS REICHERT was born in Karaganda, Kazakhstan, in 1989. He received the bachelor's and master's degrees in physics from the University of Freiburg, in 2012 and 2015, respectively, and the Ph.D. degree in physics from the Department of Radiology, Medical Physics, University Medical Center Freiburg, with a focus on MR-guided interventions.

In 2021, he became a Postdoctoral Researcher working in the field of interventional MRI. He is a member of the International Society of Magnetic Resonance in Medicine.

NIKLAS VERLOH was born in 1989. He received the degree in human medicine from the University of Regensburg.

He launched his medical career with the University Hospital Regensburg, in 2015. After completing his residency, in 2021, he was appointed as a Senior Physician for radiology with the Institute for Diagnostic Radiology, University Hospital Regensburg. His Ph.D. research delved into medical MRI imaging, mainly focusing on quantifying hepatic function. Further enhancing his academic standing, he received his Venia Legendi for his work on parenchyma analysis of the liver. Since November 2021, he has specialized in interventional radiology as a Senior Physician with the Clinic for Diagnostic and Interventional Radiology, University Medical Center Freiburg, University Hospital Freiburg. He is currently dedicated to research at the nexus of medical imaging and interventional radiology, seeking to merge these disciplines, pioneering new methods, and technologies to advance diagnostic and therapeutic procedures within the field of radiology.

Dr. Verloh is an esteemed member of several professional societies, including the Radiological Society of North America (RSNA), European Society of Radiology (ESR), Cardiovascular and Interventional Radiological Society of Europe (CIRSE), Deutsche Röntgengesellschaft (DRG), and the Deutsche Gesellschaft für Interventionelle Radiologie und minimal-invasive Therapie (DeGIR).

THOMAS LOTTNER (Member, IEEE) was born in Regensburg, Germany, in 1991. He received the bachelor's and master's degrees in physics from the University of Regensburg, in 2013 and 2016, respectively, and the Ph.D. degree from the Department of Radiology, Medical Physics, University Medical Center Freiburg, in 2023, with a focus on magnetic resonance imaging, RF simulations, MR guided interventions, and MR safety.

He is a member of the International Society of Magnetic Resonance in Medicine.

SRDJAN MILOSAVLJEVIC, photograph and biography not available at the time of publication.

MICHAEL VOGELE, photograph and biography not available at the time of publication.

WIBKE ULLER, photograph and biography not available at the time of publication.

MICHAEL BOCK was born in Helmstedt, Germany, in 1966. He studied with the University of Braunschweig and the University of Heidelberg. He received the Diploma degree in physics from the Max Planck Institute for Nuclear Physics, in 1992, the Ph.D. degree in physics from German Cancer Research Center (DKFZ), University of Heidelberg, Heidelberg, in 1995, with a focus on MRI-based velocity measurements, and the Habilitation degree in interventional MRI from the Medical Faculty, Heidelberg University, in 2009.

Since 2011, he has been a Professor of experimental radiology with the University Medical Center Freiburg, Germany. At DKFZ, he has been working, since 1996, as the Group Leader focusing on the implementation of technologies and methods for MRI-guided interventions. In 2007, he coordinated the installation of a 7 Tesla research whole body system for ultra-high field MRI in oncology. He held visiting professorships with the University of Prague and the University of Cleveland. He has published more than 200 journal articles, and supervised 11 bachelor's, 27 master's, and 40 Ph.D. theses. His work focuses on various aspects of MR imaging technologies, including for example fast real-time MRI for interventions, x-nuclear imaging with 17O, and MR imaging protocols for oncology.

Prof. Bock is a member of the International Society for Magnetic Resonance in Medicine (ISMRM) and various physics societies. Among other awards, he received the Life-Time Science Award from German Society for Medical Physics (DGMP), in 2010.

• • •